Longitudinal Stability Augmentation of Seaplanes in Planing

Keiichi Ito*† and Tom Dhaene‡

Ghent University - iMinds, Ledeberg - Ghent, 9050, Belgium

Yoshiaki Hirakawa§ and Tsugukiyo Hirayama¶

Yokohama National University, Yokohama, Kanagawa, 240-8501, Japan

Tatsumi Sakurai ‖

Hiyoh Aircraft Manufacturing and Development, Shinagawa, Tokyo, 142-0041, Japan

The towing tank experiments conducted at the Yokohama National University from November 30 to December 9 in 2005, suggested a new way of suppressing a dangerous coupled motion between heave and pitch called porpoising. This research develops on the observations made in the experiments and conducts numerical simulations to further investigate the parametric design space. Two Linear-Time-Invariant models were developed: rigid-body planing craft (conventional float planes or flying boats) and flexibly supported planing craft. The latter can simulate the new method found in the experiments for suppressing porpoising. In this study, the stability of the oscillatory motions was analyzed to see the effect of design variables to the inception of porpoising. The parametric study of flexibly supported float planes in the context of porpoising is a new contribution in the conceptual design of seaplanes.

Nomenclature

β	Deadrise angle in [degrees]
ϵ	Thrust line angle with respect to the keel line (positive upwards) in [degrees or radians]
η_3, η_5	Displacement in heave and pitch respectively from the inertial coordinate x_b, z_b
$\Re(\sigma)_{\max}$	Maximum real part of the eigenvalues of a matrix $\mathbf{K}$ as in $\dot{\mathbf{x}} = \mathbf{K}\mathbf{x}$, unit in $[1/s]$
ξ_3, ξ_5	Displacement in heave and pitch respectively from the inertial coordinate x_a, z_a
A_{ij}	Hydrodynamic added mass/moment of inertia in the direction of i due to the motion in the direction of j
B	Beam length (i.e. width) of a float in $[m]$
B_{ij}	Hydrodynamic damping coefficient in the direction of i due to the motion in the direction of j
$c_{f,b}$	Damping coefficients in the flexible support (front and back) in $[N\,s/m]$
C_{ij}	Hydrodynamic restoring force/moment coefficient in the direction of i due to the motion in the direction of j
f	Thrust line distance from CG (positive when pitch-up moment results) in $[m]$
F_{n_B}	Froude number based on the beam length defined as $U/\sqrt{gB}$, where g is gravitational acceleration
I_A	Pitching mass moment of inertia of the aircraft without the floats for the flexible-support model in $[kg\,m^2]$

*Researcher, Department of Information Technology (INTEC), Gaston Crommenlaan 8 bus 201, 9050 Ledeberg - Ghent, Belgium, and AIAA Student Member.

†Technical Specialist, Noesis Solutions, Gaston Geenslaan 11 B4, 3001 Leuven, Belgium

‡Professor, Department of Information Technology (INTEC), Gaston Crommenlaan 8 bus 201, 9050 Ledeberg - Ghent, Belgium

§Associate Professor, Department of System Integration, 79-5, Tokiwadai, Hodogayaku, Yokohama 240-8501, Japan

¶Professor Emeritus, Department of System Integration, 79-5, Tokiwadai, Hodogayaku, Yokohama 240-8501, Japan

‖Director, 1-7-1, Togoshi, Shinagawaku, Tokyo 142-0041, Japan

I_B	Pitching mass moment of inertia of the floats for the flexible-support model in $[kg\,m^2]$
I_{55}	Pitching mass moment of inertia of rigidly supported seaplane/model in $[kg\,m^2]$
$k_{f,b}$	Spring constants in the flexible support (front and back) in $[N/m]$
$l_{Af,Ab}$	Attachment locations of flexible supports on the aircraft relative to center of gravity of the aircraft in $[m]$
$l_{Bf,Bb}$	Attachment locations of flexible supports on the floats relative to center of gravity of the floats in $[m]$
l_{cg}	Longitudinal distance of center of gravity along the keel line measured from the step or transom in $[m]$
m_A	Mass of the aircraft for the flexible-support model in $[kg]$
m_B	Mass of the float for the flexible-support model in $[kg]$
N_f	Number simulation function calls
N_s	Number of simulation function calls that satisfied the stability criteria
U	Planing speed in $[m/s]$
vcg	Vertical distance of CG from the keel line in $[m]$
x_a, z_a	Inertial coordinate moving with the aircraft's CG's equilibrium position without floats, x_a pointing horizontally to the stern, z_a pointing vertically upward
x_b, z_b	Inertial coordinate moving with the aircraft's CG's equilibrium position when the supports are rigid and moving along the floats' CG's equilibrium position when the supports are flexible, x_b pointing horizontally to the stern, z_b pointing vertically upward

I. Introduction

Seaplanes and their amphibian versions have been largely a neglected type of aircraft in recent aviation except for very specific missions and in limited geographic regions. This is due to higher maintenance costs, less payload, and lower operational reliability (high waves are an additional weather hazard) compared to land based aircraft. However, recent technological advances in materials and computational capabilities along with macro-economic and ecological considerations may render this type of aircraft interesting. Point-to-point operation in coastal area could alleviate traffic congestion in urban airports and make remote islands more accessible. This in turn should help more balanced economic growth and better emergency services in smaller cities and rural areas. This paper addresses one of the drawbacks of seaplanes called porpoising which is a dynamic instability in planing seaplanes and high-speed boats.[14]

Porpoising is a coupled oscillatory motion between heaving and pitching that can manifest when seaplanes are travelling on water at planing speed (Figure 1). This motion may become unstable and can pose significant risk to the safe operation of waterborne aircraft. Traditionally, the rules of thumb in designing of hulls and physical experiments[4,6,12,15] (combined with pilot training[11,13]) have been the methods of mitigating the risk. However, the phenomenon is poorly understood and sufficient parametric studies applicable to seaplanes have not appeared in the literature. Current research aims to fill this gap. The objective is to effectively mitigate or eliminate porpoising by design.

Towing tank experiments[7] showed that the moving center of gravity aft, or employing flexible supports (between the aircraft and the floats) comparable to those of a car could improve the stability of the planing craft (Figure 2). To understand these observations, Linear-Time-Invariant models were constructed and the stability of oscillatory motions was studied. The numerical models were coherent with the experiments and two major design question were answered, namely 1) the appropriate direction to move the center of gravity when porpoising is a problem,[10] 2) whether flexible supports suppress porpoising globally or under certain conditions.

In the literature, most of the work investigating longitudinal stability of planing seaplanes is experimental. A large portion of them was conducted before the prevalence of fast personal computers (i.e., before the '70s). Parametric investigation of porpoising behavior based on numerical simulations and investigation of flexible supports for mitigation of porpoising are two contributions of this work.

II. Methods

The first step in this study was to numerically recreate at least qualitatively the observation made in the towing tank experiments. Particularly, the objective here is to confirm that the inception of porpoising

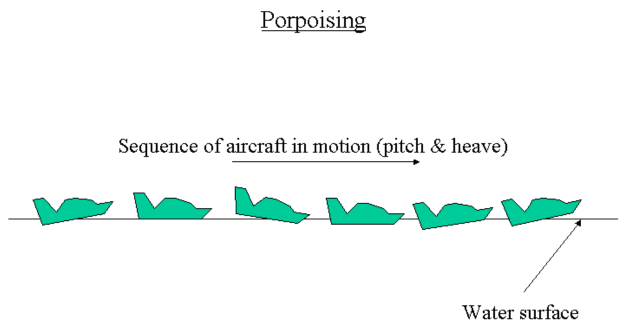

Figure 1: Schematic of porpoising

Figure 2: An implementation of the Flexible Support System in an Ultra Light Plane

occurs at approximately 5 m/s of towing speed with the original CG location, and that by moving the CG aft stabilizes the towed model. Then, observe numerically that the flexible support "stabilizes" the towed model. The second step was to explore different designs by varying parameters in the numerical model. The towed model consisted of a pair of floats in catamaran configuration and a frame on top of it (Figure 3). The frame has adjustable weights to roughly simulate the inertia characteristics of the aircraft that the float was designed for, which is a 1/3 scale Piper Cub. By changing the location of weights, one can also move the location of the CG backward or forward. In the following, the numerical model of the conventional rigid case and then the flexibly supported case are described.

For the numerical analysis, the catamaran configuration was replaced by a mono-hull representation of prismatic hull as shown in Figure 4. The transom location in this figure corresponds to the step location in the actual float. The afterbody of the float is neglected in the modelling and so is the curved front portion of the forebody of the float. The dynamic stability was computed using small perturbation analysis as presented in Faltinsen.[5] The coordinate systems employed are shown in Figure 6. For the rigidly supported case, the inertial coordinate system x_b, z_b was set to move along with the towed craft, its origin coincides with the equilibrium position of the craft's center of gravity. The x axes point to the stern of the craft. For the flexibly supported case, separate inertial coordinate systems that move along the craft were employed for above the support x_a, z_a and the float x_b, z_b. These are an approximate way to represent the dynamics (for the frame has surge component of motion that are neglected) but were done in order to facilitate the analysis. The linear system of equation for the rigidly supported case is Equation (1), and for the flexibly supported

Figure 3: Experiment with the flexible support at the towing tank of Yokohama National University

case, Equation (2). Added mass A_{ij}, damping force coefficient B_{ij}, and the restoring force coefficient C_{ij} were formulated according to chapter 8 and 9 of Faltinsen's book.[5] The numbers in subscripts $i, j \in \{3, 5\}$ denote heaving $_3$ and pitching $_5$ respectively. The first subscript $_i$ refers to the resulting force or moment direction and the second subscript $_j$ refers to the motion causing the force or moment. For example, C_{35} refers to the heaving force coefficient due to pitching motion. One can also find relevant information on the hydrodynamic forces for planing crafts in.[1, 2, 8, 10]

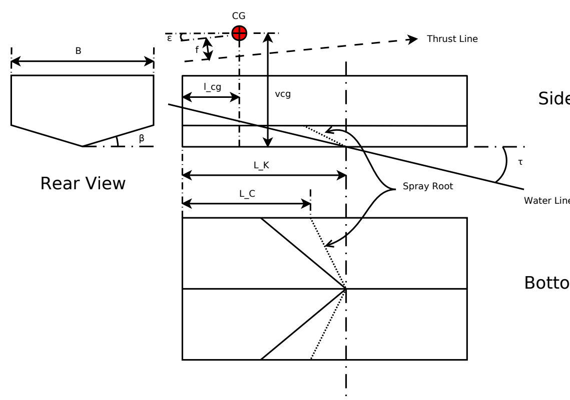

Figure 4: Diagram of planing hull cut-out.

The flexibly supported case contains additional parameters on the characteristics of the support, namely the spring constants k_f, k_b and the damping coefficients c_f, c_b. The subscripts denote their locations: $_f$ for front and $_b$ for back. Likewise, the attachment locations relative to center of gravity are denoted l_{Af}, l_{Ab} for the front and back attachment point on the aircraft side respectively, and l_{Bf}, l_{Bb} on the float side. These parameters are visualized in Figure 5. We have kept the attachment points fixed and varied the spring constants and damping coefficients in our numerical simulations.

In the rigidly supported case, we also used Self-Organizing Map Based Adaptive Sampling (SOMBAS)[9] to search for stable designs. SOMBAS is suitable for the task of searching for multiple and diverse solutions satisfying certain objective conditions. We searched for designs with negative values in maximum real part of the eigenvalues. For the two-design-variable case, we use the longitudinal distance of CG along the keel line l_{cg} measured from the step or transom, and vertical distance of CG from the keel line vcg. For the seven-design-variable case, we use the beam length B, the deadrise angle β (in degrees), the pitching moment of inertia I_{55}, the thrust line distance f from CG (positive when pitch-up moment results) and the thrust line angle with respect to the keel line (positive upwards) ϵ. Figure 4 shows a diagram describing the design variables except the inertial variable I_{55}.

$$
\begin{pmatrix} M+A_{33} & A_{35} & 0 & 0 \\ A_{53} & I_{55}+A_{55} & 0 & 0 \\ 0 & 0 & 1 & 0 \\ 0 & 0 & 0 & 1 \end{pmatrix}
\begin{pmatrix} \ddot{\eta}_3 \\ \ddot{\eta}_5 \\ \dot{\eta}_3 \\ \dot{\eta}_5 \end{pmatrix}
+
\begin{pmatrix} B_{33} & B_{35} & C_{33} & C_{35} \\ B_{53} & B_{55} & C_{53} & C_{55} \\ -1 & 0 & 0 & 0 \\ 0 & -1 & 0 & 0 \end{pmatrix}
\begin{pmatrix} \dot{\eta}_3 \\ \dot{\eta}_5 \\ \eta_3 \\ \eta_5 \end{pmatrix}
=
\begin{pmatrix} 0 \\ 0 \\ 0 \\ 0 \end{pmatrix}
\tag{1}
$$

$$
\begin{aligned}
&\begin{pmatrix}
m_A & 0 & 0 & 0 & 0 & 0 & 0 & 0 \\
0 & I_A & 0 & 0 & 0 & 0 & 0 & 0 \\
0 & 0 & 1 & 0 & 0 & 0 & 0 & 0 \\
0 & 0 & 0 & 1 & 0 & 0 & 0 & 0 \\
0 & 0 & 0 & 0 & m_B+A_{33} & A_{35} & 0 & 0 \\
0 & 0 & 0 & 0 & A_{53} & I_B+A_{55} & 0 & 0 \\
0 & 0 & 0 & 0 & 0 & 0 & 1 & 0 \\
0 & 0 & 0 & 0 & 0 & 0 & 0 & 1
\end{pmatrix}
\begin{pmatrix} \ddot{\xi}_3 \\ \ddot{\xi}_5 \\ \dot{\xi}_3 \\ \dot{\xi}_5 \\ \ddot{\eta}_3 \\ \ddot{\eta}_5 \\ \dot{\eta}_3 \\ \dot{\eta}_5 \end{pmatrix}
+ \\
&\begin{pmatrix}
c_f+c_b & c_f l_{Af}-c_b l_{Ab} & k_f+k_b & k_f l_{Af}-k_b l_{Ab} & -c_f-c_b & -c_f l_{Bf}+c_b l_{Bb} & -k_f-k_b & -k_f l_{Bf}+k_b l_{Bb} \\
c_f l_{Af}-c_b l_{Ab} & c_f l_{Af}^2+c_b l_{Ab}^2 & k_f l_{Af}-k_b l_{Ab} & k_f l_{Af}^2+k_b l_{Ab}^2 & -c_f l_{Af}+c_b l_{Ab} & -c_f l_{Af} l_{Bf}-c_b l_{Ab} l_{Bb} & -k_f l_{Af}+k_b l_{Ab} & -k_f l_{Af} l_{Bf}-k_b l_{Ab} l_{Bb} \\
-1 & 0 & 0 & 0 & 0 & 0 & 0 & 0 \\
0 & -1 & 0 & 0 & 0 & 0 & 0 & 0 \\
-c_f-c_b & -c_f l_{Af}+c_b l_{Ab} & -k_f-k_b & -k_f l_{Af}+k_b l_{Ab} & B_{33}+c_f+c_b & B_{35}+c_f l_{Bf}-c_b l_{Bb} & C_{33}+k_f+k_b & C_{35}+k_f l_{Bf}-k_b l_{Bb} \\
-c_f l_{Bf}+c_b l_{Bb} & -c_f l_{Af} l_{Bf}-c_b l_{Ab} l_{Bb} & -k_f l_{Bf}+k_b l_{Bb} & -k_f l_{Af} l_{Bf}-k_b l_{Ab} l_{Bb} & B_{53}+c_f l_{Bf}-c_b l_{Bb} & B_{55}+c_f l_{Bf}^2+c_b l_{Bb}^2 & C_{53}+k_f l_{Bf}-k_b l_{Bb} & C_{55}+k_f l_{Bf}^2+k_b l_{Bb}^2 \\
0 & 0 & 0 & 0 & -1 & 0 & 0 & 0 \\
0 & 0 & 0 & 0 & 0 & -1 & 0 & 0
\end{pmatrix}
\begin{pmatrix} \dot{\xi}_3 \\ \dot{\xi}_5 \\ \xi_3 \\ \xi_5 \\ \dot{\eta}_3 \\ \dot{\eta}_5 \\ \eta_3 \\ \eta_5 \end{pmatrix}
=
\begin{pmatrix} 0 \\ 0 \\ 0 \\ 0 \\ 0 \\ 0 \\ 0 \\ 0 \end{pmatrix}
\end{aligned}
\tag{2}
$$

III. Results

Figure 7 - Figure 9 and Figure 14 - Figure 15 are for the rigidly supported case and Figure 10 - Figure 13 are for the flexibly supported case. Nominal conditions for the calculation are as following unless otherwise specified: the planing speed $U = 6.0$ $[m/s]$, the mass of craft for the rigid case $M = 16.18$ $[kg]$ and for the flexible case $m_A = 10.79$ $[kg]$ (aircraft), $m_B = 5.39$ $[kg]$ (float), the beam length $B = 0.2$ $[m]$, the moment of inertia for the rigid case $I_{55} = 5.981$ $[kg\,m^2]$, for the flexible case $I_A = 4.351$ $[kg\,m^2]$ (aircraft), $I_B = 1.630$ $[kg\,m^2]$ (float), the length along the keel from step to center of gravity $l_{cg} = 0.104$ $[m]$, the distance of CG from the keel $v_{cg} = 0.453$ $[m]$, and the moment arm length from CG to the supports (Figure 5) are $l_{Af} = l_{Ab} = l_{Bf} = l_{Bb} = 0.2$ $[m]$. Froude number is defined based on the beam length $F_{n_B} = U/\sqrt{gB}$. The beam length B and l_{cg} are not reported in Hirakawa's paper[7] and their values are educated guesses. In the simulation, we use the half body representation. That means we half the mass and moment of inertia in the calculations, and model as a mono-hull float plane.

For plots with vertical axis showing the maximum eigenvalue $\Re(\sigma)_{\max}$ of the linear system, any positive value of the real part of the eigenvalue signifies divergence of the oscillation mode and therefore is unstable. The eigenvalues are calculated from the matrix obtained in the following way. $\mathbf{K} = \mathbf{M}^{-1}(-\mathbf{R})$, where $\mathbf{M}\dot{x} + \mathbf{R}x = 0$ and x is the state vector, where $\mathbf{M}$ and $\mathbf{R}$ represent the matrices in Equation (1) and Equation (2).

Figure 7 confirms that moving the CG backwards towards the step helps the craft to remain stable until a higher velocity. The figure shows the maximum real part of the eigenvalues $\Re(\sigma)_{\max}\sqrt{B/g}$ with respect to Froude number F_{n_B}. We kept the beam length B constant. Thus, Froude number is essentially a non-dimensionalized speed. In the towing tank experiment, divergence (porpoising) occurred at about $U = 5.0$ $[m/s]$[7] ($F_{n_B} = 3.57$) with the nominal l_{cg}/B location of 5.2. Figure 7 shows that, in the numerical simulation, planing craft with $l_{cg}/B = 0.50$ turns unstable at just under $F_{n_B} = 5.0$ and with $l_{cg}/B = 0.65$, just under $F_{n_B} = 3.5$. Note that in the physical dimensions, the two l_{cg} values differ only by 0.03 $[m]$ (or 1.95% of the float length of 1.54 $[m]$[7]) and the speed limit for stable planing changed by 2.10 $[m/s]$ (or 42.8% difference). Thus, the planing speed U at which the craft turns unstable is very sensitive to the CG location. Considering the fact that values for B and l_{cg} are only approximately known, the numerical results are very reasonable in light of the experimental evidence.

The trim angles τ corresponding to the two l_{cg} values with respect to F_{n_B} are shown in Figure 8. The trim angles are found by driving the moment equation to have near zero residue moment. This is done using Brent's method [3, Ch.3-4] implemented in Scipy optimize module of the Python programming language. One can let the solutions to have small residues so that the trim angles found can be used as a small perturbation in the subsequent eigenvalue computations.

Figure 9 indicates that the desirable direction of moving the CG ,i.e. forward or backward, to stabilize an unstable planing condition depends on the current value of l_{cg}. There is a band of l_{cg} values at which a non-decaying oscillation manifests with positive $\Re(\sigma)_{\max}\sqrt{B/g}$. This band of instability increases in width as F_{n_B} increases from 2.86 to 5.71 as seen in Figure 9a to Figure 9c. The contour plots show that the sensitivity of the stability to changes in vcg is not as marked as changes in l_{cg}. A small portion of the design space near the transom or very small value of l_{cg} generates stable designs, and most float planes have this configuration to facilitate the pitch up at the moment of take off. This means that to make the planing stable, it is a good idea to shift the CG aft. However, once airborne, it is better to have CG forward to have enough "static margin" for a stable flight.

Figure 10 checks whether the two simulation codes, one for the rigid-body case and the other for the flexibly supported case, agree if the flexible support's spring were extremely stiff. The plot shows $\Re(\sigma)_{\max}\sqrt{B/g}$ with respect to F_{n_B}. The two lines agree very well.

Figure 11 - Figure 13 show the effectiveness of the flexible support in mitigating unstable oscillations. However, as can be noted from the sharp rise in the real part of eigenvalues at high Froude numbers, it is not a globally stabilizing solution. Inadequate damping in the flexible supports can worsen the stability of the seaplane compared with the conventional rigidly supported ones as seen in Figure 11a or in Figure 11b. This suggests that the damper should be designed carefully in such a way that no divergent oscillation modes occur in the planing speeds of the aircraft. Figure 12 shows that if only one of either front or back support is made flexible, it is the back support that is effective in mitigating instabilities. Similarly, if damping is applied to either the front or the back support (that are both flexible), it is the damping of the back support that is more effective (Figure 13). These results show some similarity with the flutter stability phenomena

in Aeroelasticity, in which the elastic axis location of the wing affects the divergence speed.

Figure 14 shows a contour plot of $\Re(\sigma)_{\max}\sqrt{B/g}$ with respect to l_{cg} and vcg along with sampled points by SOMBAS in two-design-variable case. SOMBAS was set to search feasible designs requiring $\Re(\sigma)_{\max} < 0$. The sampled points that satisfies that condition are shown along with the final location of the training samples for Self-Organizing Map (SOM). The distribution of the training samples indicates the finite sample representation of the feasible region around which further sampling in the subsequent iterations are expected produce further space filling effect of the feasible design space, i.e. further stable designs. In this trivial case (because we already have the contour plot), we see that SOMBAS sampled diverse combinations of l_{cg} and v_{cg} filling out the stable domain. This feasible region search capability is useful when the design space is in higher dimensions (many design variables) and full-factorial design (or grid sampling) becomes too expensive.

Figure 15a shows the scatter plot matrix of the seven design variable case. N_f is the number of designs (experiments) computed by SOMBAS and N_s is the number designs that satisfy the condition, i.e., $\Re(\sigma)_{\max} < 0$. The lower triangular cells show the absolute values of correlation coefficients. Again, it clearly shows the unstable "band" for l_{cg} at the top row of the scatter plot matrix. Other parameter does not show clear unfeasible regions. Further restriction was applied by setting $\Re(\sigma)_{\max} < -0.3$ and the results are shown in Figure 15b. It shows some new trends. For example, vcg tends to lower value as the eigenvalue becomes more negative. On the other hand the beam length B tends to larger value as the eigenvalue becomes more negative. The l_{cg} concentrates between 0.6 and 1.1, and vcg tends to low values as l_{cg} becomes longer.

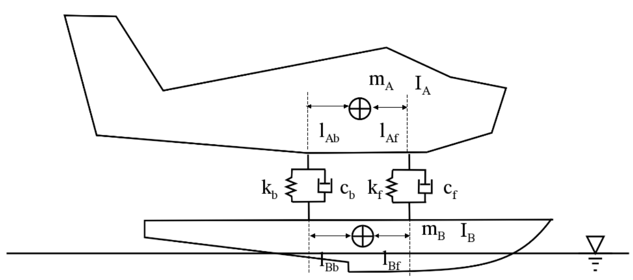

Figure 5: Schematic of a float plane with the flexible support

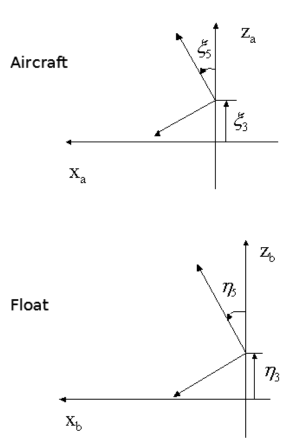

Figure 6: Coordinate system for the Small Perturbation Method

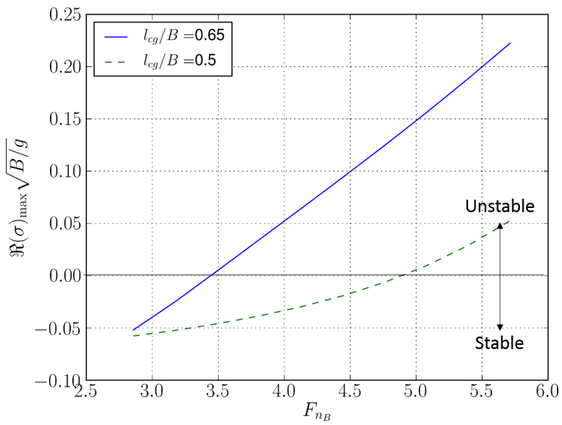

Figure 7: Porpoising mitigation by moving the CG aft.

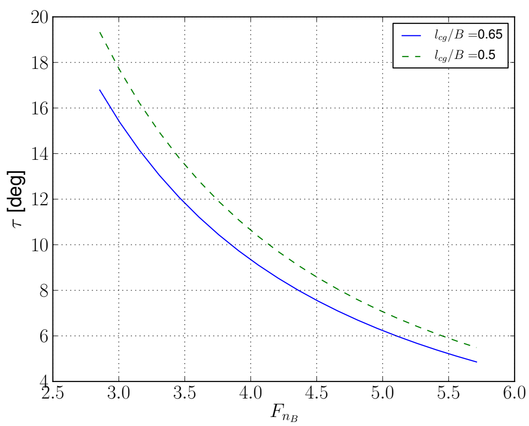

Figure 8: Trim angle of the simulated model with respect to Frounde number F_{n_B}

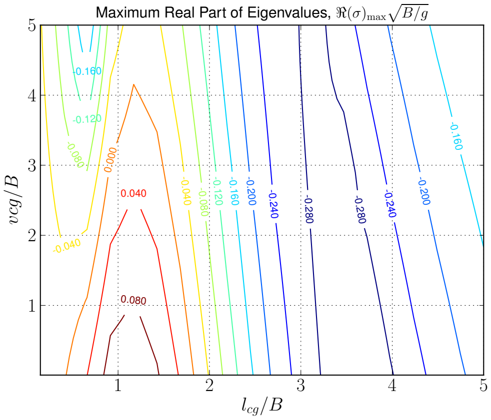

(a) $F_{n_B} = 2.86$

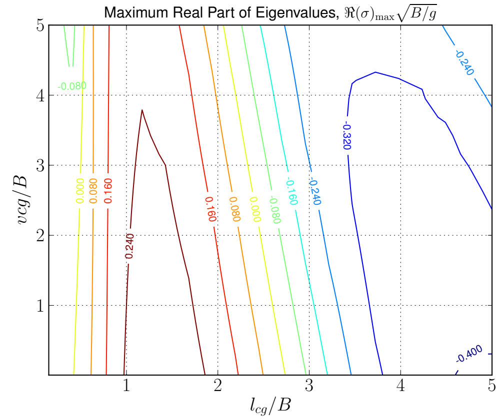

(b) $F_{n_B} = 4.28$

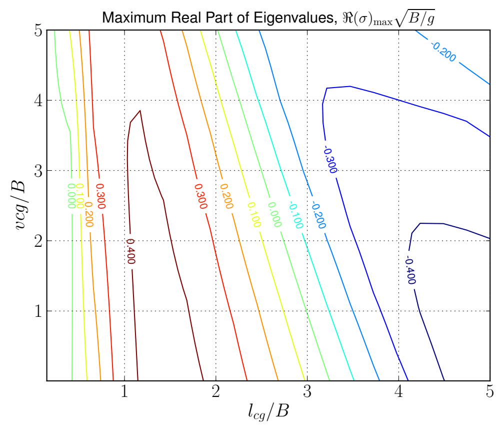

(c) $F_{n_B} = 5.71$

Figure 9: Stability with respect to l_{cg} and v_{cg}. $\Re(\sigma)_{\max}\sqrt{B/g} < 0$ are stable designs.

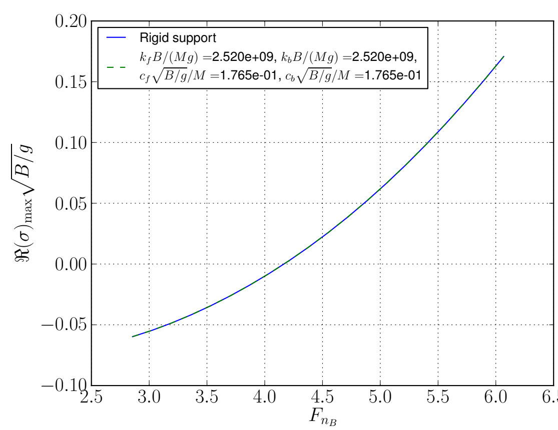

Figure 10: Comparison of stability results in the rigid-body formulation and the flexible-support formulation with very stiff springs

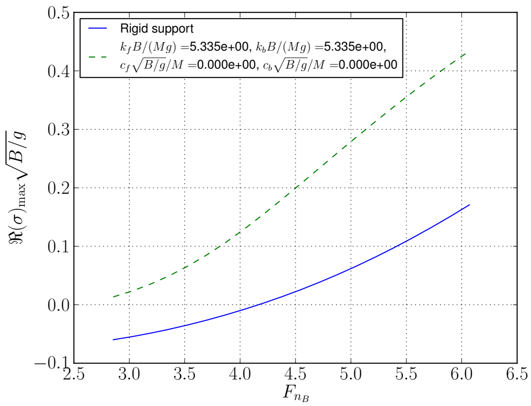

(a) No damping

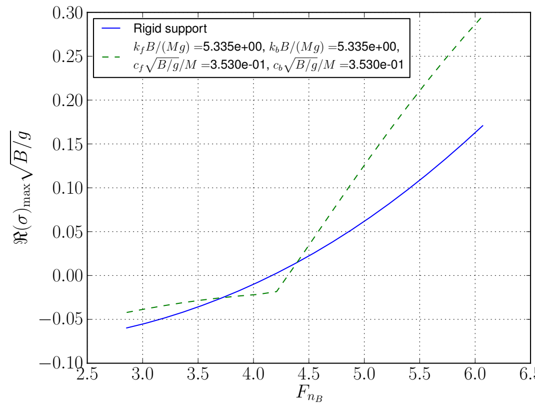

(b) $c_{f,b} = 20$ $[N\, s/m]$

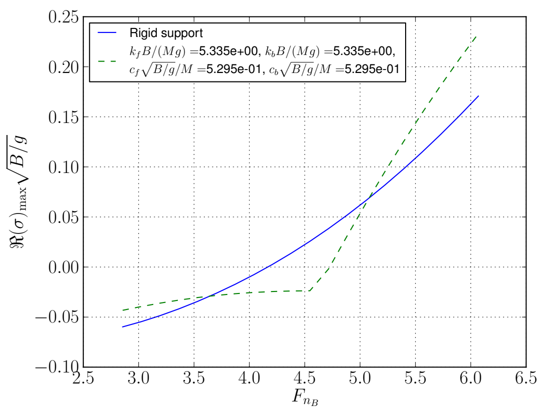

(c) $c_{f,b} = 30$ $[N\, s/m]$

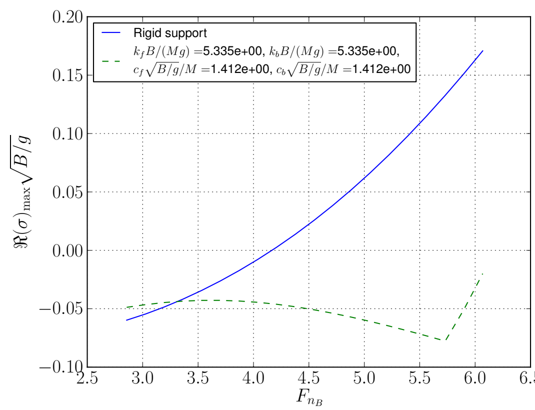

(d) $c_{f,b} = 80$ $[N\, s/m]$

Figure 11: Comparison of longitudinal stability between rigidly supported case and flexibly supported case. Fixed spring constant $k_{f,b} = 2117[N/m]$ with various damping coefficients.

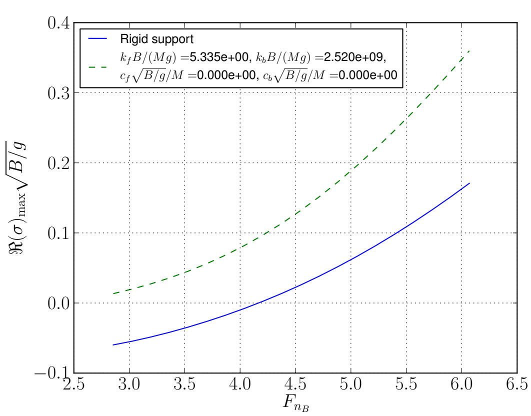

(a) Flexible front support, no damping

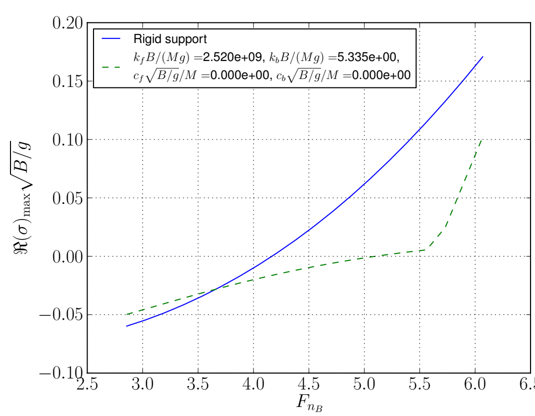

(b) Flexible back support, no damping

Figure 12: Comparison of longitudinal stability between the rigidly supported case and the flexibly supported case. Spring applied only to the front k_f or to the back k_b, with no damping applied

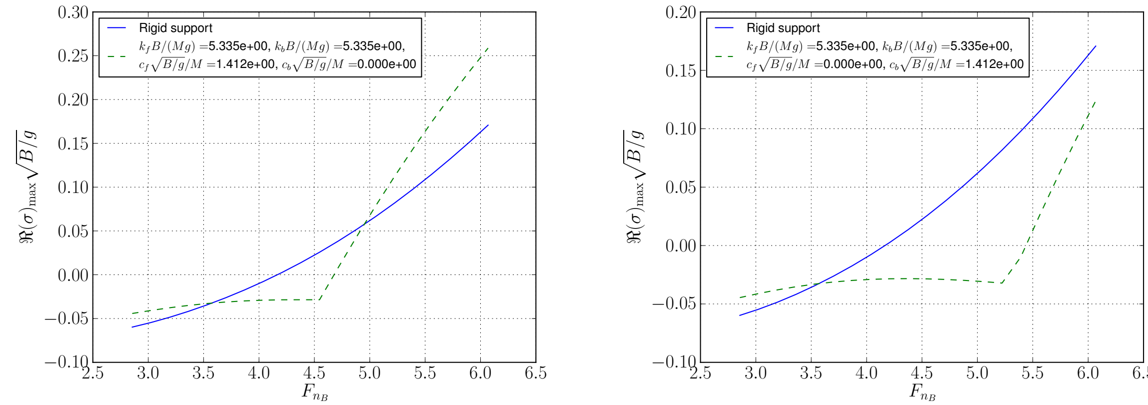

(a) Applying damping only to the front support

(b) Applying damping only to the back support

Figure 13: Comparison of longitudinal stability between the rigidly supported case and the flexibly supported case. Fixed spring constant $k_{f,b} = 2117[N/m]$, with damping of 80 $[N\,s/m]$ applied to either the front or the back support

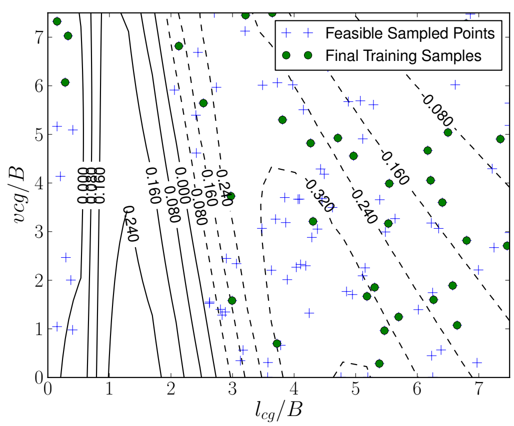

Figure 14: SOMBAS sampling stable combinations of l_{cg} and vcg at $F_{n_B} = 4.28$

IV. Discussions

It is desirable to conduct further experiments to improve the quality of the model by calibration and further numerical model refinement. The hull geometry and the flexible-support model employed in this research were very simple. Inclusion of the afterbody of the float (the portion after the step) may create another planing surface at larger pitch angles, and this may create another instability. Further sophistication in the flexible-support model, including their control may render further insights and new opportunities.

In the current study, the CG location (l_{cg} and vcg) and the pitching moment of inertia (I_{55},$I_{A,B}$) were treated independently. However, in reality, they are not. If you change the CG location, so do the moments of inertia. Thus, care must be taken to interpret the results in this paper where both variables are treated independently.

In this study the aerodynamic effects are not considered. However, seaplanes receive substantial lift force at planing speeds and the elevator provides a means to control the pitch angle. Thus the aerodynamics may have a substantial effect on the planing characteristics of a seaplane. The inclusion of the aerodynamic effects will be the next step in the development of the numerical simulation of the planing seaplanes.

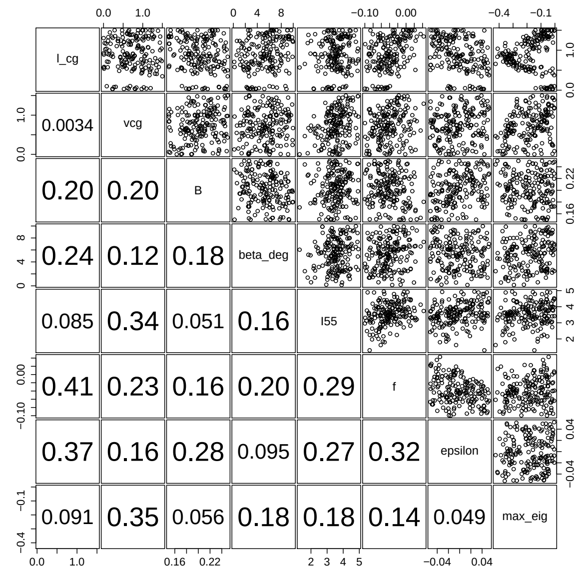

(a) Maximum eigenvalues of oscillation modes less than 0, ($N_f = 289, N_s = 181$)

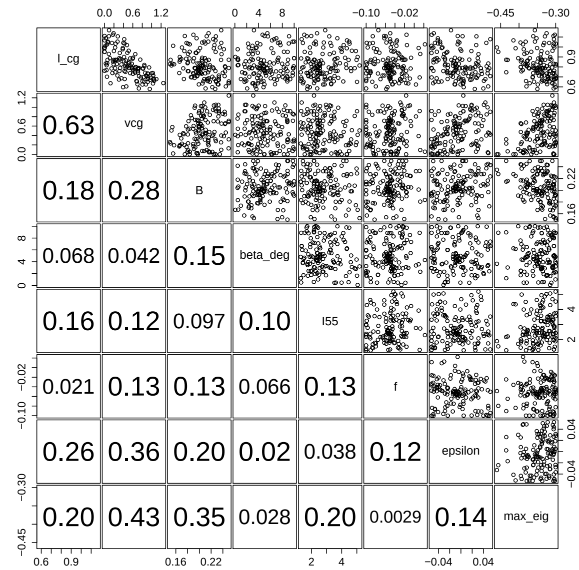

(b) Maximum eigenvalues of oscillation modes less than -0.3, ($N_f = 504, N_s = 135$)

Figure 15: Scatter Matrix showing distribution of feasible designs at $F_{n_B} = 4.28$

V. Conclusion

The numerical analysis of the Linear-Time-Invariant model revealed useful information to the questions posed. The computation shows that whether one should move the center of gravity backward or forward will depend on the position of center of gravity with respect to the step of the planing hull. If a flexible support is employed one may postpone the inception of porpoising to a much higher Froude number. The simulation results indicate that damping coefficients in the flexible supports play an important role and the range of planing speed will determine their values. The damping in the hind support was more effective than the damping in the front support. These numerical results can be used to conduct more dedicated physical experiments to quantitatively assess the numerical models and confirm physical phenomena. Furthermore, aerodynamic effects must be taken into account. These will constitute the future work of this study along with the parametric optimization of the system.

VI. Acknowledgment

Keiichi Ito has been funded by the Institute for the Promotion of Innovation through Science and Technology (IWT) through the Baekeland Mandate program in the research and development of SOMBAS. His research has also been funded by the Interuniversity Attraction Poles Programme BESTCOM initiated by the Belgian Science Policy Office. The undergoing project of developing innovative seaplanes (project managed by Tatsumi Sakurai and the members of Hiyoh Aircraft Manufacturing and Development Co. and Aeromarine Systems Cooperation Association) is an endeavour supported by many dedicated and enthusiastic volunteers.

References

[1]Serge Abrate. Hull slamming. *Applied Mechanics Reviews*, 64(6):060803–1 – 060803–35, November 2011.

[2]James M. Benson and Anton Freihofner. Methods and charts for computing stability derivatives of a v-bottom planing surface. Technical Report NACA ARR 3L08, National Advisory Committee for Aeronautics, Langley Memorial Aeronautical Laboratory, 1943.

[3]Richard P. Brent. *Algorithms for Minimization Without Derivatives.* Prentice-Hall, Englewood Cliffs, NJ, 1973.

[4]Jr. Charles L. Shuford. A theoretical and experimental study of planing surfaces including effects of cross section and

plan form. Report 1355, National Advisory Committee for Aeronautics, 1958.

[5]Odd M. Faltinsen. *Hydrodynamics of High-Speed Marine Vehicles*. Cambridge University Press, 2005.

[6]H. M. Garner. Porpoising test on a model of a flying boat hull. Reports and Memoranda 1492, Marine Aircraft Experimental Establishment, March 1932.

[7]Yoshiaki Hirakawa, Takehiko Takayama, Asuka Kosaki, Hiromitsu Kikuchi, Tsugukiyo Hirayama, and Tatsumi Sakurai. Model experiment of a suppression-system for wave impact and porpoising phenomena. *Conference Proceedings of The Japan Society of Naval Architects and Ocean Engineers (in Japanese)*, 3:239–242, 2006.

[8]Yoshiho Ikeda and Toru Katayama. Porpoising oscillation of very-high-speed marine craft. *Philosophical Transactions of The Royal Society, Series A*, 358(1771):1905–1915, 2000.

[9]Keiichi Ito, Tom Dhaene, Naji El Masri, Roberto d'Ippolito, and Joost Van de Peer. Self-organizing map based adaptive sampling. In *Proceedings of 5th International Conference on Experiments/Process/System Modeling/Simulation/Optimization (5th IC-EpsMsO)*, volume II, pages 504 – 513, Athens, Greece, July 3 - 6 2013. ISBN:978-618-80527-2-7 or 978-618-80527-0-3.

[10]Alexander Klemlin, John D. Pierson, and Edmund M. Storer. An introduction to seaplane porpoising. *Journal of the Aeronautical Sciences*, 6(8):1905–1915, June 1939.

[11]Burke Mees. *Notes of a Seaplane Instructor*. Aviation Supplies & Academics, Newcatle, Washington, 1998.

[12]John B. Parkinson. Appreciation and determination of the hydrodynamic qualities of seaplanes. Technical Note 1290, National Advisory Committee for Aeronautics, Washington, May 1947.

[13]Dale De Remer. *Water Flying Concepts: an Advanced Text on Wilderness Water Flying*. Aviation Supplies & Academics, Newcastle, Washington, 2nd edition, 1990.

[14]Darrol Stinton. Aero-marine design and flying qualities of floatplanes and flying-boats. *Aeronautical Journal*, pages 97–127, March 1987.

[15]K. M. Tomaszewski. Hydrodynamic design of seaplane floats. Current papers, Ministry of Supply Aeronautical Research Council, 1950.